NANO LETTERS

pubs.acs.org/NanoLett

Letter

# Enhanced Electron Transport in Nonconjugated Radical Oligomers Occurs by Tunneling

Ying Tan, Jialing Li, Songsong Li, Hao Yang, Teng Chi, Stephen B. Shiring, Kangying Liu, Brett M. Savoie, Bryan W. Boudouris,* and Charles M. Schroeder*

Cite This: *Nano Lett.* 2023, 23, 5951−5958

Read Online

ACCESS | Metrics & More | Article Recommendations | Supporting Information

**ABSTRACT:** Incorporating temperature- and air-stable organic radical species into molecular designs is a potentially advantageous means of controlling the properties of electronic materials. However, we still lack a complete understanding of the structure−property relationships of organic radical species at the molecular level. In this work, the charge transport properties of (2,2,6,6-tetramethylpiperidin-1-yl)oxyl (TEMPO) radical-containing nonconjugated molecules are studied using single-molecule charge transport experiments and molecular modeling. Importantly, the TEMPO pendant groups promote temperature-independent molecular charge transport in the tunneling region relative to the quenched and closed-shell phenyl pendant groups. Results from molecular modeling show that the TEMPO radicals interact with the gold metal electrodes near the interface to facilitate a high-conductance conformation. Overall, the large enhancement of charge transport by incorporation of open-shell species into a single nonconjugated molecular component opens exciting avenues for implementing molecular engineering in the development of next-generation electronic devices based on novel nonconjugated radical materials.

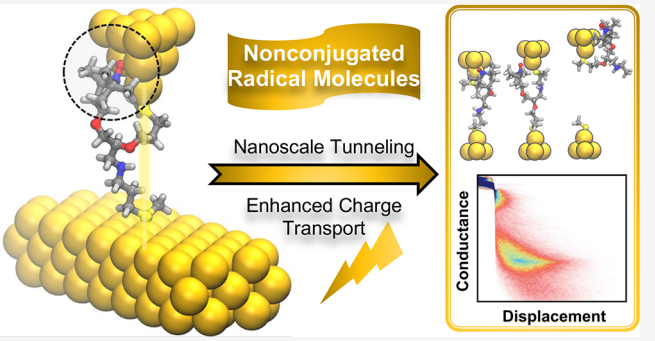


**KEYWORDS:** *scanning tunneling microscope−break junction (STM-BJ), single-molecule charge transport, open-shell molecules, nonconjugated radical electronics*



Radical polymers (i.e., macromolecules where pendant radical species are attached to a nonconjugated backbone) have emerged as new functional materials for applications in electronic devices such as batteries, memristors, and diodes due to their unique redox, optical, and electronic properties.[1−10] Organic radical species are open-shell systems with unpaired electrons that have attracted extensive interest in controlling molecular electronics properties such as the Kondo effect and magnetoresistive phenomena.[11−14] However, the fundamental charge transport mechanisms of organic radical species are not fully understood. Recent advances in single-molecule characterization have enabled the study of charge transport mechanisms in organic materials at the single-molecule level using experimental techniques such as the mechanically controllable break junction (MCBJ)[15] and the scanning tunneling microscope−break junction (STM-BJ).[16] By directly measuring charge transport at the single-molecule level, these techniques establish a direct connection between the intrinsic charge transport properties and molecular architecture, which can be addressed by incorporating versatile functional groups and by designing different chemical structures. In this way, single-molecule approaches allow for an understanding of intramolecular charge transport separately from the contributing effects of nearby molecules, thereby enabling a fundamental understanding of electron transport at the molecular level.[17−20]

The integration of open-shell species into nonconjugated systems allows for the molecular engineering of mechanical properties separately from functional properties by altering the polymer backbone and introducing radical species as pendant groups, respectively. Broadly, this approach leads to a larger design space compared with conjugated systems. In addition, the structural flexibility and stability of these materials aid in materials processing for device applications.[8,21] Prior work that used individual radical molecules as active electronic units in break-junction platforms focused on the interactions between localized electronic moments and conduction electrons[22] and reported radical-enhanced transport.[23−26] However, these efforts primarily focused on spin delocalized radicals,[27,28]

**Received:** March 14, 2023
**Revised:** June 25, 2023
**Published:** June 29, 2023

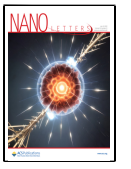

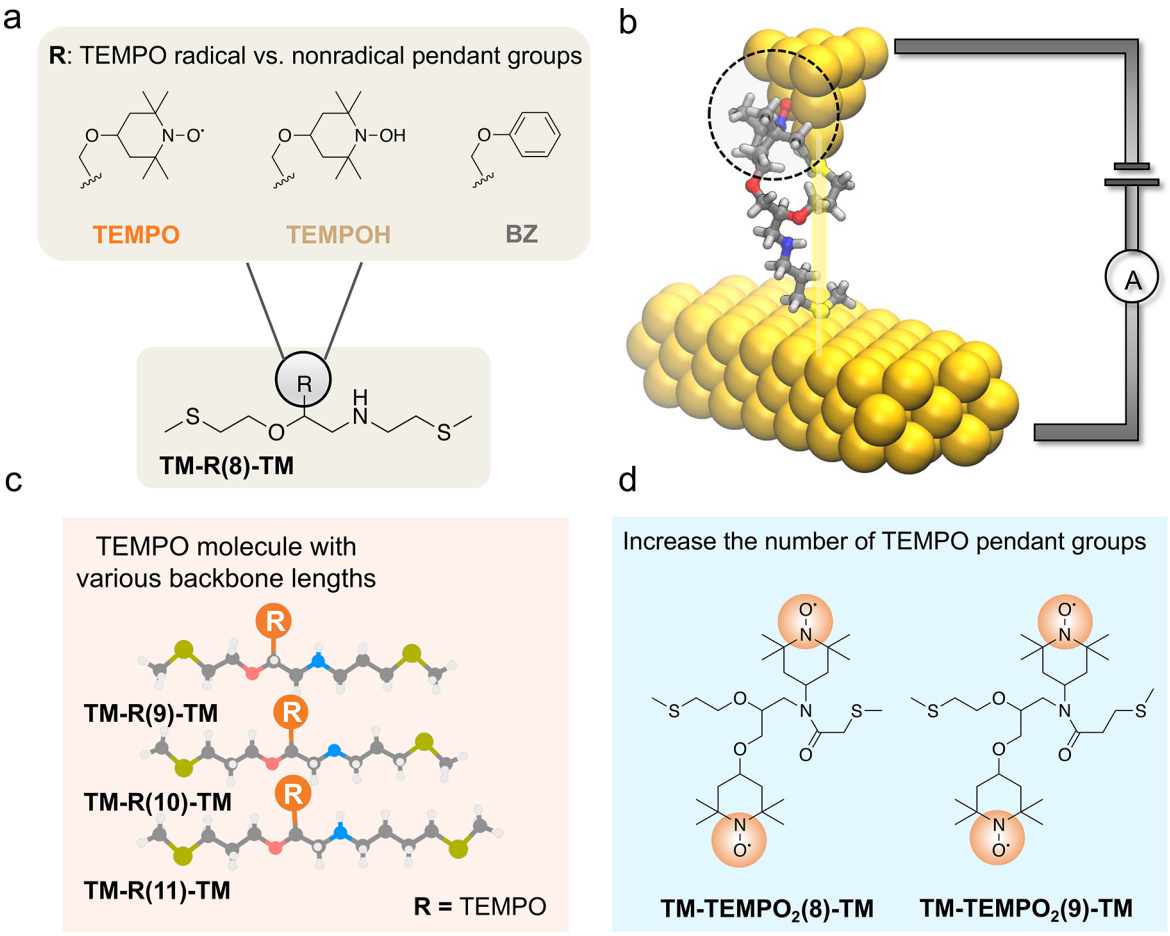


**Figure 1.** Schematic of the molecular series evaluated in this work. (a) Molecular structures of radical, quenched radical control, and closed-shell control molecules. (b) Simulated conformation of the TEMPO radical assisting transport in a single-molecule junction platform. (c) Single TEMPO containing molecules with various backbone lengths studied in this work. (d) TEMPO-dimer thiolated molecules with 8 or 9 heavy atoms of the backbone studied in this work.

conjugated backbone structures,[12,29,30] or both.[25] The fundamental mechanisms of charge transport in radical-based molecular electronics with conjugated backbones do not directly translate to nonconjugated systems. For these reasons, it is essential to characterize the electronic properties of nonconjugated radical materials at the molecular level to elucidate the fundamental mechanisms of charge transport in nonconjugated open-shell chemistries. Here, we use a combination of the synthetic design of radical chemistries, single-molecule techniques, and molecular modeling to understand the nanoscale charge transport mechanisms of nonconjugated radical molecules containing unpaired electrons.

The charge transport properties of a series of molecules consisting of radical-attached heteroalkyl building blocks are evaluated. Particular attention is focused on understanding the role of isolated radical chemistries in intramolecular charge transport. The 2,2,6,6-tetramethylpiperidin-1-oxyl (TEMPO) radical group was implemented as the open-shell moiety due to its stability and facile synthesizability. Uniquely, the frontier orbital of the unpaired electron on the TEMPO radical does not delocalize into the backbone; that is, the radical group is electrically isolated from the backbone transport channel. Surprisingly, single-molecule charge transport experiments reveal that despite being attached to the nonconjugated backbone, the TEMPO radical enhances the molecular conductance of the nonconjugated molecule. In addition, TEMPO-containing single molecules of discretely varying backbone lengths exhibit higher conductance than pure alkyl chains, while exhibiting a similar conductance decay profile as a function of the number of carbon units in the backbone chain. Temperature-dependent measurements suggest that tunneling is the dominant transport mechanism over hopping, given the nanoscale dimensions of the molecules. Results from molecular modeling suggest that radical−gold interactions at the electrodes promote high conductance conformations. To further explore the effect of radical density on charge transport at the single molecular level, TEMPO diradical molecules were also investigated and found to exhibit conductance comparable to that of the one-TEMPO-containing molecule. These key findings on microscopic conduction highlight that radical-induced molecular conformations and electrode interactions significantly contribute to the charge transport behavior of nonconjugated radical materials.

A series of TEMPO-containing thiolated derivatives were synthesized and characterized using proton ($^1$H) and carbon ($^{13}$C) nuclear magnetic resonance (NMR) spectroscopy and high-resolution mass spectrometry (Figures S1−S15). The building blocks consisted of pendant TEMPO groups attached to a heteroalkyl chain with anchoring thiomethyl (TM) moieties at both termini, resulting in conductive molecular wires suitable for STM-BJ experiments (Figure 1a,b).


https://doi.org/10.1021/acs.nanolett.3c00978
Nano Lett. 2023, 23, 5951−5958

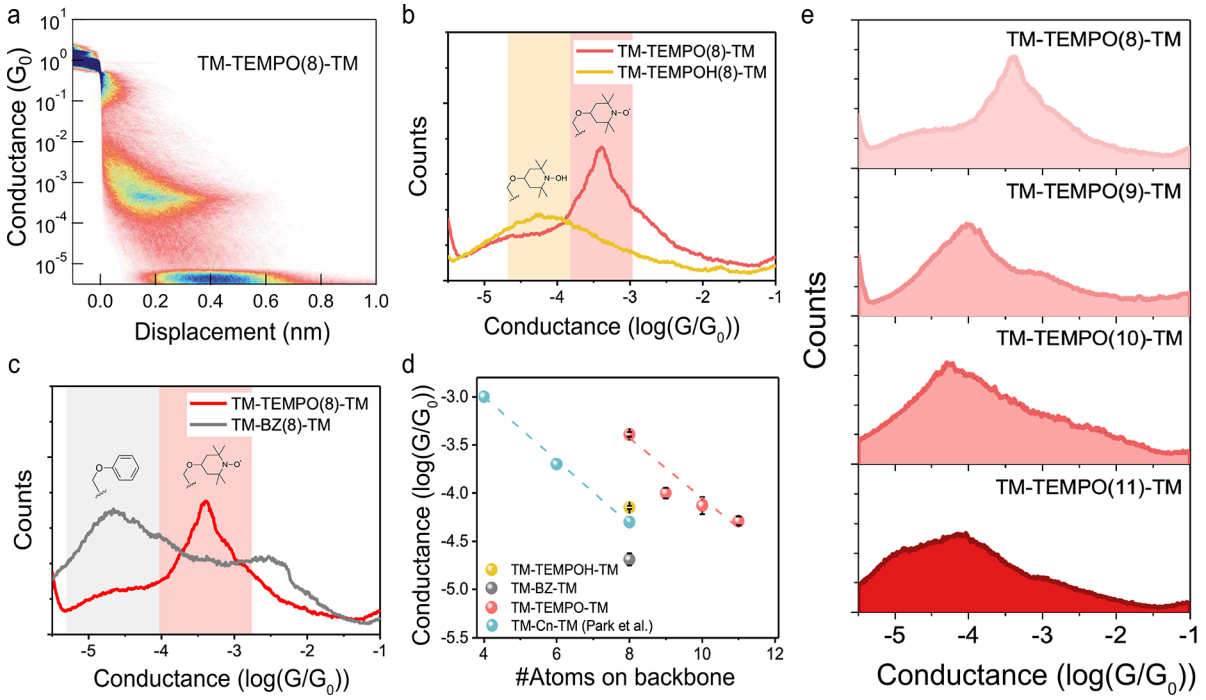


**Figure 2.** Molecular conductance of single-radical containing molecules. (a) Two-dimensional (2D) conductance versus displacement histogram of **TM-TEMPO(8)-TM** in 1,2,4-trichlorobenzene (TCB) constructed from 5000 individual traces at 250 mV applied bias without data selection. (b) Comparison of one-dimensional (1D) conductance histograms between radical **TM-TEMPO(8)-TM** and quenched **TM-TEMPOH(8)-TM** molecule. (c) Comparison of 1D conductance histograms between radical **TM-TEMPO(8)-TM** and neutral phenyl analogue **TM-BZ(8)-TM** molecule. (d) Conductance of all single-TEMPO, TEMPOH, and phenyl-containing molecules plotted against the number of heavy atoms in the nonconjugated backbone shown on a semilog scale. Each conductance point is calculated from the peak value of the Lorentz fit to the corresponding 1D conductance histogram. Dashed lines are fits to the experimental data on the semilog scale. Data shown for pure alkane chains of different lengths as a comparison adapted from ref 37. Error bars represent the standard deviation from three subsamples of each measurement. (e) 1D conductance histograms of **TM-TEMPO(*x*)-TM** ($x$ = 8−10) molecules compiled from at least 5000 individual traces without data selection.

Specifically, a series of TEMPO-containing monomers [**TM-TEMPO(*x*)-TM**] were created, where $x$ denotes a backbone length of 8−11 heteroatoms between anchor groups (Figure 1c). To establish the role of the radical moiety on conductance, the **TM-TEMPOH(8)-TM** molecule with a quenched radical and the **TM-BZ(8)-TM** molecule with a closed-shell phenyl-substituted group were synthesized as controls (Figure 1a). To further extend this design paradigm, a TEMPO-containing dimer series [**TM-TEMPO$_2$(*x*)-TM**] with a backbone length of 8 and 9 heteroatoms between anchor groups was also synthesized (Figure 1d). Electron paramagnetic resonance (EPR) spectra showed the expected triplet splitting pattern for the monomer series and quintet for the dimer series due to the unpaired electron coupling to nitrogen nuclei with a spin of 1 (Figure S16). The dimer molecule showed hyperfine coupling lines with a spacing of 0.79 mT, corresponding to half of the monomer's spacing of 1.57 mT. In this way, this well-defined set of materials facilitated the systematic characterization of nanoscale transport in nonconjugated radical molecules.

Single-molecule experiments effectively captured the nanoscale effect on charge transport when incorporating pendant open shell species along nonconjugated backbones. Initial experiments showed that the introduction of radical-containing species resulted in an order of magnitude increase in molecular conductance compared to that of the closed-shell control molecules. In particular, the charge transport properties of the open-shell species **TM-TEMPO(*x*)-TM** ($x$ = 8−11) were characterized using a custom-built STM-BJ instrument, as previously described (Supporting Information).[19,31,32] Figures 2a,b show the 2D molecular conductance histogram of **TM-TEMPO(8)-TM**, which has a clear conductance plateau around 4.1 × $10^{-4}$ $G_0$ (where $G_0 = 2e^2/h$ is the quantum unit of conductance) with a junction length of approximately 0.9 nm, after correcting for the 5 Å snap-back distance.[33,34] In contrast, quenched **TM-TEMPOH(8)-TM** shows a 10-fold lower molecular conductance (Figure 2b). The higher conductance peak for **TM-TEMPO(8)-TM** also indicates a more stable molecule junction, as discussed in the Molecular Modeling section (Figures 2b and S17a). A closed-shell control molecule, **TM-BZ(8)-TM**, with a phenyl group replacing TEMPO on the same nonconjugated backbone chain was also characterized using STM-BJ. The major conductance peak of **TM-BZ(8)-TM** is around 2.0 × $10^{-5}$ $G_0$, which is approximately 20 times smaller than that of **TM-TEMPO-(8)-TM** (Figures 2c and S17b). A shoulder peak around 4.0 × $10^{-3}$ $G_0$ was also observed, which likely arises due to the shorter conductance pathway arising from van der Waals interactions between the conjugated phenyl group and the gold electrode.[35,36]

A series of additional experiments on TEMPO-containing molecules with different backbone lengths and control molecules further showed an enhancement in molecular conductance for open-shell radical-containing molecules. Molecules with different spacer lengths (i.e., with 9, 10, and 11 heavy atoms in the backbone chains between the two anchor groups) were first characterized using STM-BJ to understand the backbone-length dependence of charge trans-


https://doi.org/10.1021/acs.nanolett.3c00978
Nano Lett. 2023, 23, 5951−5958

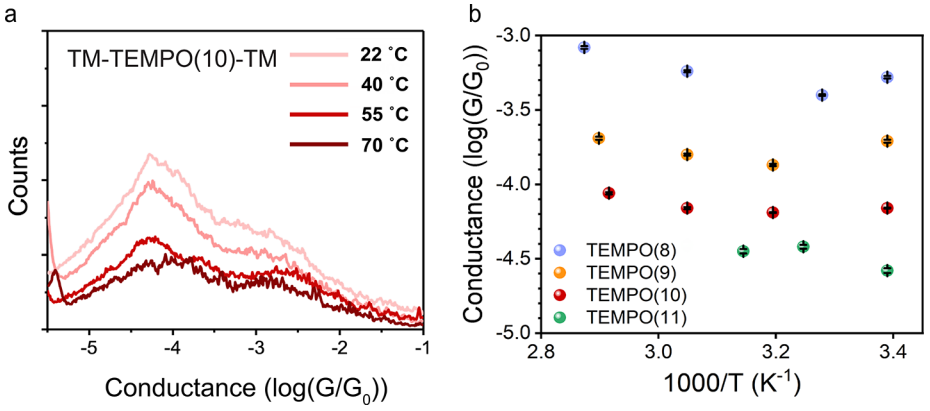


**Figure 3.** Temperature-dependent single-molecule junction measurements of one-TEMPO-containing molecules. (a) 1D conductance histograms of **TM-TEMPO(10)-TM** in TCB at 22, 40, 55, and 70 °C constructed from 5000 individual traces for each temperature at 250 mV applied bias without data selection. (b) Most probable single-molecule conductance of TM-**TEMPO(*x*)-TM** ($x$ = 8−11) plotted against different temperatures. Error bars represent the standard deviation from subsamples of each measurement.

port on single TEMPO containing molecules. All three molecules formed stable molecular junctions with decreasing conductance at $1 \times 10^{-4}$, $7.4 \times 10^{-5}$, and $5.1 \times 10^{-5}$ $G_0$, respectively, as the backbone length increases (Figures 2e and S18). Notably, a short plateau appears in the 2D conductance histograms for all four TEMPO-containing molecules, possibly resulting from different molecular junction geometries during stretching or different backbone interactions with substrate electrodes, wherein the secondary amine along the molecular backbone may competitively bind with the gold electrode to form a shorter junction. This short plateau is also observed in intermediate products (**TM-TEMPO**) containing only one thiomethyl anchor group as evaluated via STM-BJ (Figure S19). Furthermore, both the 1D and 2D molecular conductance histograms of these one-anchor intermediates display conductance peaks that are qualitatively different from their two-anchor counterparts (Figure S19). In addition, TEMPO-$NH_2$ reveals that the interaction between TEMPO and the gold electrode alone is not strong enough to form a stable linkage (Figure S20). Taken together, the dominant molecular conductance features identified here correspond to end-to-end linkages of near fully stretched conformations. To summarize, the molecular conductance of TEMPO-containing molecules is plotted together with the control molecules containing quenched TEMPOH and the phenyl-substituted **TM-BZ(8)-TM** in comparison to alkyl chains terminated with the same anchor group, as reported in prior work (Figure 2d). These results highlight that TEMPO-containing molecules show higher end-to-end junction conductance peak values than all of the control counterparts.[37]

Temperature-dependent STM-BJ measurements on open shell radical molecules supported this guiding vision as well.[38,39] Figure 3a shows the 1D molecular conductance histograms of **TM-TEMPO(10)-TM** in TCB solution measured at 22, 40, 55, and 70 °C at 250 mV applied bias. Across this temperature range, the conductance peaks remain at the same conductance values. It is worth noting that the peak intensity decreases at higher temperatures due to the weakened junction stability from increasing molecular conformational changes upon activation by temperature. Figure 3b shows the peak molecular conductance of **TM-TEMPO(*x*)-TM** ($x$ = 8−11) at different temperatures, indicating that the charge transport in TEMPO-containing molecules is independent of temperature over the range evaluated here (Figure S21). Given the weak electronic coupling between TEMPO radicals, the open-shell species are often modeled as hopping sites in prior studies.[40,41] However, the experimental results suggest that tunneling transport is nevertheless the dominant charge transport mechanism over the range of backbone lengths and temperatures evaluated in this work.[42−44]

The conductance−length relationship for the TEMPO-containing molecules was fit with a coherent tunneling model such that $G \propto e^{-\beta L}$, where $\beta$ corresponds to the conductance decay constant and $L$ corresponds to the number of atoms between two anchor groups in the backbone (Figure 2d). The conductance decay parameter $\beta$ for TEMPO molecules was found to be approximately 0.31 ± 0.06 per backbone atom, whereas the $\beta$ value for alkyl chains is 0.45 ± 0.02 per carbon atom.[37] Within the range of molecular lengths investigated in this work, it may appear that **TM-TEMPO(9−11)-TM** exhibits a slightly smaller conductance decay slope than that of **TM-TEMPO(8)-TM**. However, the contour lengths for all of these molecules are significantly smaller than the previously reported transition length from tunneling to hopping transport.[45,46] This is consistent with a tunneling mechanism for the four single-TEMPO-containing molecules reported in this work. We note that the conductance decay constant for **TM-TEMPO(9−11)-TM** is slightly smaller than that of **TM-TEMPO(8−9)-TM**, which is potentially due to the increased conformational flexibility of the longer molecules or the smaller change in end-to-end molecular length from the relaxed optimized geometries calculated by DFT (Figure S22). Overall, the molecular conductance of TM-TEMPO-TM molecules is larger than that of the carbon chains with the same number of backbone atoms, but the conductance decreases at a similar rate as a function of backbone length. This is consistent with the idea that the TEMPO pendant group is electronically decoupled from the backbone, and thus, the enhanced molecular conductance could arise from differences in molecular conformations induced by introducing the radical pendant group, such as the differences in binding configuration with the electrodes.

Molecular conformations induced by interactions between the TEMPO pendant group and the electrode surface contributed to the increased tunneling transport efficiency. Molecular dynamics and conformational searches[47−49] were performed to study molecular conformations of single-


https://doi.org/10.1021/acs.nanolett.3c00978
Nano Lett. 2023, 23, 5951−5958

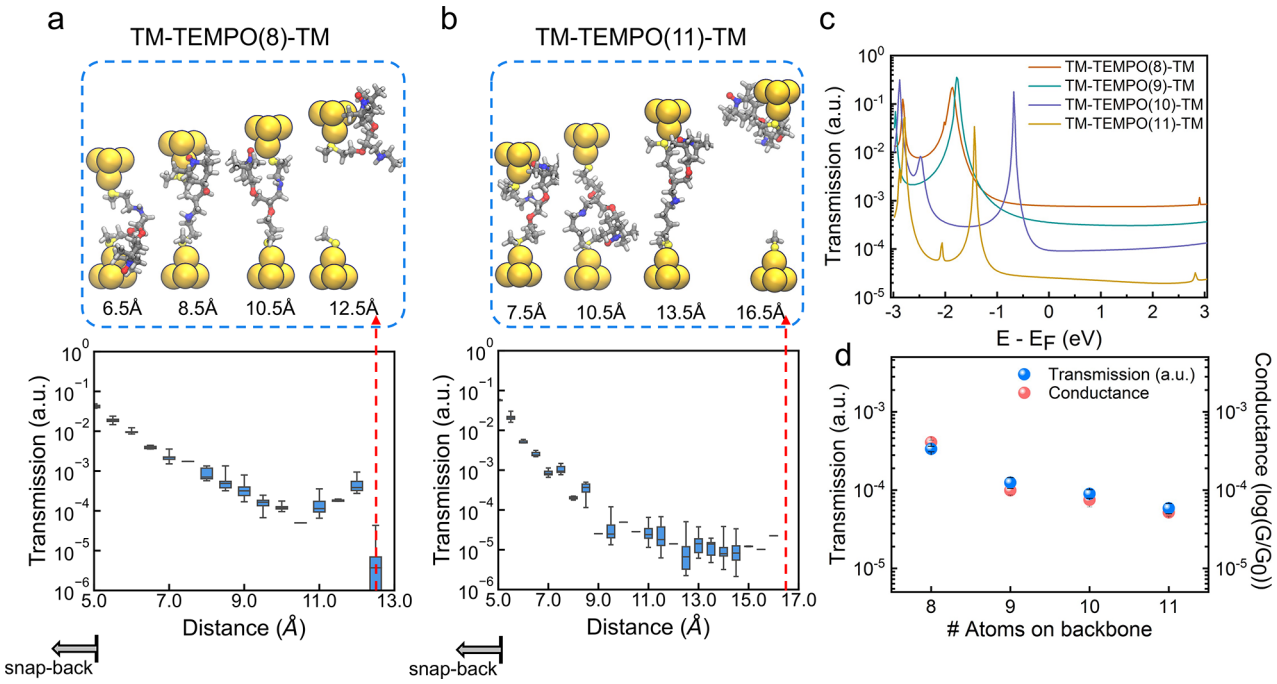


**Figure 4.** Molecular simulations of geometries and transmission properties of single-molecule junctions formed by one-TEMPO-containing molecules. Lowest energy conformations and transmission curves at interval stretching distances of single molecules of two backbone lengths (a) **TM-TEMPO(8)-TM** and (b) **TM-TEMPO(11)-TM**. The nitroxide head of the TEMPO radical tends to attach to one of the gold electrodes. The starting distance of the transmission curve was reported starting from 5 Å due to the snap-back effect. (c) Simulated transmission of the lowest energy conformer of molecules investigated with a stretching distance of 9 Å. (d) Comparison of the simulated average transmission and experimentally measured mean conductance.

molecule junctions formed by TEMPO-containing molecules (Figures 4 and S23). Visualization of the spin density confirms that the TEMPO radical is localized at the nitroxide head, not along the main molecular backbone pathway (Figure S26). Results from molecular modeling show that during junction formation and breakage, a molecular conformation with the nitroxide head of the TEMPO radical attached to one of the gold electrodes was frequently observed (Figure 4a,b). These radical−electrode conformations typically showed the lowest energies, suggesting that the binding energy between the radical and electrode was >6 kcal $mol^{-1}$ across the energy window of conformations explored. The pendant radical group interacts with the electrode, until the interaction is disrupted at large electrode−electrode separations.

Results from transport calculations showed that the transmission curve[50,51] exhibits an exponential decay with the elongation of the junction, followed by a sudden drop at junction breakage (i.e., manifested as a sulfur−gold bond break) at 12.5 Å for the **TM-TEMPO(8)-TM** molecule and at 16.5 Å for the **TM-TEMPO(11)-TM** molecule (Figure 4a,b). However, experimentally measured conductance traces of molecules with backbone lengths longer than 9 heavy atoms showed increased heterogeneity, which likely arises due to changes in molecular conformations, bonding geometries, and molecule−electrode contacts. Complementary to the observed heterogeneity in single-molecule conductance experiments, a statistically representative transmission value was obtained to characterize the charge transport capabilities in simulation. Simulation results focused on energetically stabilized configurations and included an explicit definition of the breaking distance to characterize the charge transport capabilities. At the same stretching length, the transmission level at the Fermi level generally declines with the increase of backbone length (Figure 4c). Moreover, the simulated average transmission closely matched the statistically obtained conductance from experiments (Figure 4d). The addition of radical groups leads to increased alignment of the frontier molecular orbitals[52] with the electrode Fermi energy (Figure S25). However, results from the transport simulations show that the average transmission of radical and nonradical molecules are comparable (Figures 4 and S24). For these reasons, our results suggest that the distinct conformation of the radical molecule and interactions between the TEMPO group and the electrode give rise to the enhanced conductance in TEMPO-containing molecules. Together, the combined experimental and simulation results reveal how conformations modulate radical-enhanced charge transport in single nonconjugated molecules.

The incorporation of TEMPO diradical moieties onto the heteroatom alkyl chains did not result in a significant improvement in the single-molecule junction performance, despite an increase in radical density. Prior work on radical-containing polymers suggests a strong density dependence of conductivity on the radical loading.[53] We therefore hypothesized that the addition of the radical species would enhance the charge transport at the single-molecule level. Thus, a TEMPO diradical thiolated molecule with an eight-atom-long backbone **TM-TEMPO$_2$(8)-TM** was synthesized. Single-molecule charge transport measurements were performed at 250 and 500 mV applied bias (Figure S27). In contrast to the anticipated result, the weak signal intensity in the 2D conductance versus displacement histogram suggests a low probability of forming stable molecular junctions due to the proximity of the bulky TEMPO group to the thiomethyl


https://doi.org/10.1021/acs.nanolett.3c00978
Nano Lett. 2023, 23, 5951−5958

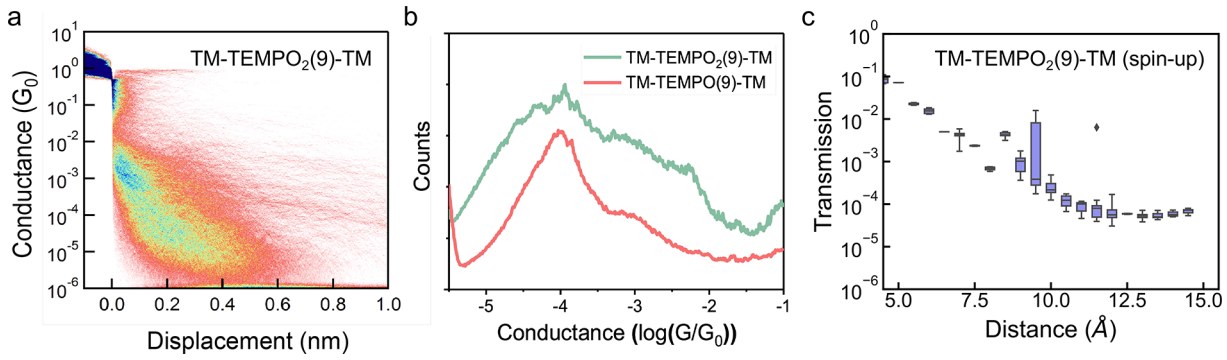


**Figure 5.** Experimental and simulation results of single-molecule junction studies focused on TEMPO diradical molecules. (a) 2D conductance versus displacement histogram of **TM-TEMPO$_2$(9)-TM** in TCB at room temperature constructed from 5000 individual traces for each temperature at 250 mV applied bias without data selection. (b) 1D conductance histograms of **TM-TEMPO$_2$(9)-TM** in comparison with **TM-TEMPO(9)-TM**. (c) Spin-up transmission curve of the diradical molecule with varied pulling distance.

anchor group, which potentially hinders robust binding interactions between the anchor group and the gold electrode (Figure S28). Therefore, a modified version of **TM-TEMPO$_2$(9)-TM** was synthesized with an additional carbon linker between the amide group and the thiomethyl anchor group to increase the distance between the TEMPO group and the anchor group. Single-molecule conductance results show that **TM-TEMPO$_2$(9)-TM** forms more stable junctions with a slightly longer junction displacement compared to its single-TEMPO counterpart (Figure 5a). However, the conductance peak is relatively unchanged, around $1.3 \times 10^{-4}$ $G_0$, with a broader peak width on the 1D conductance histogram compared to **TM-TEMPO(9)-TM** (Figure 5b). The temperature-independent feature of the diradical molecule is consistent with the idea that the dominant charge transport mechanism is temperature-independent tunneling (Figure S29), which is not directly related to the degeneracy caused by unpaired electrons. Molecular modeling was performed to validate the experimental results of charge transport in TEMPO diradical containing molecules. Similar to the results from single TEMPO-containing molecules, an exponential decay of transmission with distance was observed for the diradical system (i.e., spin-up transmission in Figure 5c and spin-down transmission in Figure S30c). For the low-energy conformational ensemble, two representative configurations were observed (Figure S30a), with one of the TEMPO groups attached to the electrode accounting for 70% of the total configurations. Results from molecular simulations show that in the dominant conformation the electronic couplings between the TEMPO radicals are exceedingly small, falling in a minimal range between 0.0001 and 0.01 eV, and therefore contribute negligibly to the overall tunneling efficiency and make intramolecular hopping highly unlikely (Figure S31).[40,54] In addition, the simulated plateaus of both spin-up and spin-down transmission were of the same order of magnitude as the monomeric version of the same length. Apparently, the addition of a second radical group did not significantly improve the charge transport, in part due to the low probability of both radicals being attached to electrodes. Although rarely observed, some molecular conformations showed a notable difference in spin-up and spin-down transmission (Figure S30b), indicating a spin injection barrier channel, which was atypical but possible.[12] This diradical-character-induced effect partly explains the broad distribution of experimentally measured conductance.

In conclusion, single-molecule junction measurements were performed on a series of radical-containing molecules with thiolated, nonconjugated backbone structures. A significant increase in the molecular conductance was observed for the open-shell-bearing molecules relative to the analogous closed-shell or quenched radical species molecules. Radical-attached molecules exhibited higher conductance values than non-pendant-group-attached alkyl chains with similar decay constants $\beta$ as a function of molecular length. When diradicals were incorporated into the single-molecule junction, molecular conductance was similar to that of single TEMPO-containing molecules. The weak temperature dependence of the molecular conductance further supports a tunneling transport mechanism rather than hopping for these materials. Molecular modeling revealed that the main transmission channel is through the nonconjugated backbone and that charge transport is facilitated by radical−electrode interactions. Overall, this work highlights the role of radical-assisted tunneling in open-shell molecules and suggests potential strategies and design rules to mediate electronic interactions in open-shell materials.

## ■ ASSOCIATED CONTENT

### Supporting Information

The Supporting Information is available free of charge at https://pubs.acs.org/doi/10.1021/acs.nanolett.3c00978.

Additional details on general experimental procedures; synthesis and characterization of TEMPO-bearing molecules and control molecules; scanning tunneling microscope-break junction experiments; computational methods and other supplementary experimental and simulation data (PDF)

## ■ AUTHOR INFORMATION

### Corresponding Authors

**Bryan W. Boudouris** − *Charles D. Davidson School of Chemical Engineering, Purdue University, West Lafayette, Indiana 47907, United States; Department of Chemistry, Purdue University, West Lafayette, Indiana 47907, United States;* orcid.org/0000-0003-0428-631X; Email: boudouris@purdue.edu

**Charles M. Schroeder** − *Department of Chemical and Biomolecular Engineering, University of Illinois at Urbana−Champaign, Urbana, Illinois 61801, United States; Beckman Institute for Advanced Science and Technology,*



https://doi.org/10.1021/acs.nanolett.3c00978
Nano Lett. 2023, 23, 5951−5958

*Department of Materials Science and Engineering, and Department of Chemistry, University of Illinois at Urbana−Champaign, Urbana, Illinois 61801, United States; Joint Center for Energy Storage Research, Argonne National Laboratory, Lemont, Illinois 60439, United States;* orcid.org/0000-0001-6023-2274; Email: cms@illinois.edu

### Authors

**Ying Tan** − *Charles D. Davidson School of Chemical Engineering, Purdue University, West Lafayette, Indiana 47907, United States;* orcid.org/0000-0002-7762-0836

**Jialing Li** − *Department of Chemical and Biomolecular Engineering, University of Illinois at Urbana−Champaign, Urbana, Illinois 61801, United States; Beckman Institute for Advanced Science and Technology, University of Illinois at Urbana−Champaign, Urbana, Illinois 61801, United States; Joint Center for Energy Storage Research, Argonne National Laboratory, Lemont, Illinois 60439, United States*

**Songsong Li** − *Beckman Institute for Advanced Science and Technology and Department of Materials Science and Engineering, University of Illinois at Urbana−Champaign, Urbana, Illinois 61801, United States; Joint Center for Energy Storage Research, Argonne National Laboratory, Lemont, Illinois 60439, United States*

**Hao Yang** − *Beckman Institute for Advanced Science and Technology and Department of Materials Science and Engineering, University of Illinois at Urbana−Champaign, Urbana, Illinois 61801, United States*

**Teng Chi** − *Department of Chemistry, Purdue University, West Lafayette, Indiana 47907, United States*

**Stephen B. Shiring** − *Charles D. Davidson School of Chemical Engineering, Purdue University, West Lafayette, Indiana 47907, United States*

**Kangying Liu** − *Department of Chemistry, Purdue University, West Lafayette, Indiana 47907, United States*

**Brett M. Savoie** − *Charles D. Davidson School of Chemical Engineering, Purdue University, West Lafayette, Indiana 47907, United States;* orcid.org/0000-0002-7039-4039

Complete contact information is available at: https://pubs.acs.org/10.1021/acs.nanolett.3c00978

### Author Contributions

Y.T. and J.L. contributed equally to this work.

### Notes

The authors declare no competing financial interest.

## ■ ACKNOWLEDGMENTS

The authors thank Prof. Dr. Carmen Herrmann for granting permission to use the transport code ARTAIOS. Molecular synthesis and simulations were supported by the Air Force Office of Scientific Research (AFOSR) under support provided by the Organic Materials Chemistry Program (Grant: FA9550-23-1-0240, Program Manager: Dr. Kenneth Caster). Experiments on single-molecule electronic measurements were supported by the Joint Center for Energy Storage Research (JCESR), an Energy Innovation Hub funded by the U.S. Department of Energy, Office of Science, Basic Energy Sciences. The work on mass spectroscopy was supported in part by the Research Instrumentation Center in the Department of Chemistry at Purdue University.

## ■ REFERENCES

(1) Zhang, K.; Monteiro, M. J.; Jia, Z. Stable Organic Radical Polymers: Synthesis and Applications. *Polym. Chem.* **2016**, *7* (36), 5589−5614.

(2) Wingate, A. J.; Boudouris, B. W. Recent Advances in the Syntheses of Radical-Containing Macromolecules. *J. Polym. Sci. Part A Polym. Chem.* **2016**, *54* (13), 1875−1894.

(3) Chen, Z. X.; Li, Y.; Huang, F. Persistent and Stable Organic Radicals: Design, Synthesis, and Applications. *Chem.* **2021**, *7* (2), 288−332.

(4) Mukherjee, S.; Boudouris, B. W. *Organic Radical Polymers: New Avenues in Organic Electronics*; Springer: 2017.

(5) Wang, S.; Easley, A. D.; Lutkenhaus, J. L. 100th Anniversary of Macromolecular Science Viewpoint: Fundamentals for the Future of Macromolecular Nitroxide Radicals. *ACS Macro Lett.* **2020**, *9*, 358−370.

(6) Wilcox, D. A.; Agarkar, V.; Mukherjee, S.; Boudouris, B. W. Stable Radical Materials for Energy Applications. *Annu. Rev. Chem. Biomol. Eng.* **2018**, *9*, 83−103.

(7) Ji, L.; Shi, J.; Wei, J.; Yu, T.; Huang, W. Air-Stable Organic Radicals: New-Generation Materials for Flexible Electronics? *Adv. Mater.* **2020**, No. 190815, 32.

(8) Tan, Y.; Hsu, S. N.; Tahir, H.; Dou, L.; Savoie, B. M.; Boudouris, B. W. Electronic and Spintronic Open-Shell Macromolecules, Quo Vadis? *J. Am. Chem. Soc.* **2022**, *144* (2), 626−647.

(9) Hansen, K. A.; Blinco, J. P. Nitroxide Radical Polymers-A Versatile Material Class for High-Tech Applications. *Polym. Chem.* **2018**, *9* (13), 1479−1516.

(10) Xie, Y.; Zhang, K.; Yamauchi, Y.; Oyaizu, K.; Jia, Z. Nitroxide Radical Polymers for Emerging Plastic Energy Storage and Organic Electronics: Fundamentals, Materials, and Applications. *Mater. Horizons* **2021**, *8* (3), 803−829.

(11) Hayakawa, R.; Karimi, M. A.; Wolf, J.; Huhn, T.; Zöllner, M. S.; Herrmann, C.; Scheer, E. Large Magnetoresistance in Single-Radical Molecular Junctions. *Nano Lett.* **2016**, *16* (8), 4960−4967.

(12) Zöllner, M. S.; Nasri, R.; Zhang, H.; Herrmann, C. Design Considerations for Oligo(p-Phenyleneethynylene) Organic Radicals in Molecular Junctions. *J. Phys. Chem. C* **2021**, *125* (2), 1208−1220.

(13) Mitra, G.; Low, J. Z.; Wei, S.; Francisco, K. R.; Deffner, M.; Herrmann, C.; Campos, L. M.; Scheer, E. Interplay between Magnetoresistance and Kondo Resonance in Radical Single-Molecule Junctions. *Nano Lett.* **2022**, *22* (14), 5773−5779.

(14) Baum, T. Y.; Fernández, S.; Peña, D.; Van Der Zant, H. S. J. Magnetic Fingerprints in an All-Organic Radical Molecular Break Junction. *Nano Lett.* **2022**, *22* (20), 8086−8092.

(15) Reed, M. A.; Zhou, C.; Muller, C. J.; Burgin, T. P.; Tour, J. M. Conductance of a Molecular Junction. *Science (80-.)* **1997**, *278* (5336), 252−254.

(16) Venkataraman, L.; Klare, J. E.; Tam, I. W.; Nuckolls, C.; Hybertsen, M. S.; Steigerwald, M. L. Single-Molecule Circuits with Well-Defined Molecular Conductance. *Nano Lett.* **2006**, *6* (3), 458−462.

(17) Xiang, D.; Wang, X.; Jia, C.; Lee, T.; Guo, X. Molecular-Scale Electronics: From Concept to Function. *Chem. Rev.* **2016**, *116* (7), 4318−4440.

(18) Zhang, J.; Kuznetsov, A. M.; Medvedev, I. G.; Chi, Q.; Albrecht, T.; Jensen, P. S.; Ulstrup, J. Single-Molecule Electron Transfer in Electrochemical Environments. *Chem. Rev.* **2008**, *108* (7), 2737−2791.

(19) Li, S.; Jira, E. R.; Angello, N. H.; Li, J.; Yu, H.; Moore, J. S.; Diao, Y.; Burke, M. D.; Schroeder, C. M. Using Automated Synthesis to Understand the Role of Side Chains on Molecular Charge Transport. *Nat. Commun.* **2022**, *13* (1), 1−8.

(20) Yu, H.; Li, S.; Schwieter, K. E.; Liu, Y.; Sun, B.; Moore, J. S.; Schroeder, C. M. Charge Transport in Sequence-Defined Conjugated Oligomers. *J. Am. Chem. Soc.* **2020**, *142* (10), 4852−4861.

(21) Ko, J.; Yu, I.; Jeon, S. Y.; Sohn, D.; Im, S. G.; Joo, Y. Mapping Out the Nonconjugated Organic Radical Conductors via Chemical or Physical Pathways. *JACS Au* **2022**, *2* (9), 2089−2097.

(22) Low, J. Z.; Kladnik, G.; Patera, L. L.; Sokolov, S.; Lovat, G.; Kumarasamy, E.; Repp, J.; Campos, L. M.; Cvetko, D.; Morgante, A.; et al. The Environment-Dependent Behavior of the Blatter Radical at the Metal−Molecule Interface. *Nano Lett.* **2019**, *19* (4), 2543−2548.
(23) Li, J.; Pudar, S.; Yu, H.; Li, S.; Moore, J. S.; Rodríguez-López, J.; Jackson, N. E.; Schroeder, C. M. Reversible Switching of Molecular Conductance in Viologens Is Controlled by the Electrochemical Environment. *J. Phys. Chem. C* **2021**, *125* (40), 21862−21872.
(24) Yuan, L.; Franco, C.; Crivillers, N.; Mas-Torrent, M.; Cao, L.; Sangeeth, C. S.; Rovira, C.; Veciana, J.; Nijhuis, C. A. Chemical Control over the Energy-Level Alignment in a Two-Terminal Junction. *Nat. Commun.* **2016**, *7* (1), 1−10.
(25) Liu, J.; Zhao, X.; Al-Galiby, Q.; Huang, X.; Zheng, J.; Li, R.; Huang, C.; Yang, Y.; Shi, J.; Manrique, D. Z.; et al. Radical-Enhanced Charge Transport in Single-Molecule Phenothiazine Electrical Junctions. *Angew. Chem.* **2017**, *129* (42), 13241−13245.
(26) Naghibi, S.; Sangtarash, S.; Kumar, V. J.; Wu, J. Z.; Judd, M. M.; Qiao, X.; Gorenskaia, E.; Higgins, S. J.; Cox, N.; Nichols, R. J. Redox-Addressable Single-Molecule Junctions Incorporating a Persistent Organic Radical. *Angew. Chem., Int. Ed.* **2022**, DOI: 10.1002/anie.202116985.
(27) Li, L.; Low, J. Z.; Wilhelm, J.; Liao, G.; Gunasekaran, S.; Prindle, C. R.; Starr, R. L.; Golze, D.; Nuckolls, C.; Steigerwald, M. L.; et al. Highly Conducting Single-Molecule Topological Insulators Based on Mono- and Di-Radical Cations. *Nat. Chem.* **2022**, *14* (9), 1061−1067.
(28) Frisenda, R.; Gaudenzi, R.; Franco, C.; Mas-Torrent, M.; Rovira, C.; Veciana, J.; Alcon, I.; Bromley, S. T.; Burzurí, E.; Van Der Zant, H. S. J. Kondo Effect in a Neutral and Stable All Organic Radical Single Molecule Break Junction. *Nano Lett.* **2015**, *15* (5), 3109−3114.
(29) Herrmann, C.; Solomon, G. C.; Ratner, M. A. Designing Organic Spin Filters in the Coherent Tunneling Regime. *J. Chem. Phys.* **2011**, DOI: 10.1063/1.3598519.
(30) Chen, H.; Jiang, F.; Hu, C.; Jiao, Y.; Chen, S.; Qiu, Y.; Zhou, P.; Zhang, L.; Cai, K.; Song, B.; et al. Electron-Catalyzed Dehydrogenation in a Single-Molecule Junction. *J. Am. Chem. Soc.* **2021**, *143* (22), 8476−8487.
(31) Li, S.; Yu, H.; Li, J.; Angello, N.; Jira, E. R.; Li, B.; Burke, M. D.; Moore, J. S.; Schroeder, C. M. Transition between Nonresonant and Resonant Charge Transport in Molecular Junctions. *Nano Lett.* **2021**, *21* (19), 8340−8347.
(32) Yu, H.; Li, J.; Li, S.; Liu, Y.; Jackson, N. E.; Moore, J. S.; Schroeder, C. M. Efficient Intermolecular Charge Transport in π-Stacked Pyridinium Dimers Using Cucurbit[8]Uril Supramolecular Complexes. *J. Am. Chem. Soc.* **2022**, *144* (7), 3162−3173.
(33) Moreno-García, P.; Gulcur, M.; Manrique, D. Z.; Pope, T.; Hong, W.; Kaliginedi, V.; Huang, C.; Batsanov, A. S.; Bryce, M. R.; Lambert, C.; et al. Single-Molecule Conductance of Functionalized Oligoynes: Length Dependence and Junction Evolution. *J. Am. Chem. Soc.* **2013**, *135* (33), 12228−12240.
(34) Hong, W.; Manrique, D. Z.; Moreno-García, P.; Gulcur, M.; Mishchenko, A.; Lambert, C. J.; Bryce, M. R.; Wandlowski, T. Single Molecular Conductance of Tolanes: Experimental and Theoretical Study on the Junction Evolution Dependent on the Anchoring Group. *J. Am. Chem. Soc.* **2012**, *134* (4), 2292−2304.
(35) Aradhya, S. V.; Frei, M.; Hybertsen, M. S.; Venkataraman, L. Van Der Waals Interactions at Metal/Organic Interfaces at the Single-Molecule Level. *Nat. Mater.* **2012**, *11* (10), 872−876.
(36) Wei, Y.; Li, L.; Greenwald, J. E.; Venkataraman, L. Voltage-Modulated van Der Waals Interaction in Single-Molecule Junctions. *Nano Lett.* **2023**, *23*, 567.
(37) Park, Y. S.; Whalley, A. C.; Kamenetska, M.; Steigerwald, M. L.; Hybertsen, M. S.; Nuckolls, C.; Venkataraman, L. Contact Chemistry and Single-Molecule Conductance: A Comparison of Phosphines, Methyl Sulfides, and Amines. *J. Am. Chem. Soc.* **2007**, *129* (51), 15768−15769.
(38) Hines, T.; Diez-Perez, I.; Hihath, J.; Liu, H.; Wang, Z. S.; Zhao, J.; Zhou, G.; Müllen, K.; Tao, N. Transition from Tunneling to Hopping in Single Molecular Junctions by Measuring Length and Temperature Dependence. *J. Am. Chem. Soc.* **2010**, *132* (33), 11658−11664.
(39) Ie, Y.; Okamoto, Y.; Inoue, T.; Tone, S.; Seo, T.; Honda, Y.; Tanaka, S.; Lee, S. K.; Ohto, T.; Yamada, R.; et al. Highly Planar and Completely Insulated Oligothiophenes: Effects of π-Conjugation on Hopping Charge Transport. *J. Phys. Chem. Lett.* **2019**, *10* (12), 3197−3204.
(40) Tan, Y.; Casetti, N. C.; Boudouris, B. W.; Savoie, B. M. Molecular Design Features for Charge Transport in Nonconjugated Radical Polymers. *J. Am. Chem. Soc.* **2021**, *143* (31), 11994−12002.
(41) Sato, K.; Ichinoi, R.; Mizukami, R.; Serikawa, T.; Sasaki, Y.; Lutkenhaus, J.; Nishide, H.; Oyaizu, K. Diffusion-Cooperative Model for Charge Transport by Redox-Active Nonconjugated Polymers. *J. Am. Chem. Soc.* **2018**, *140* (3), 1049−1056.
(42) Magoga, M.; Joachim, C. Minimal Attenuation for Tunneling through a Molecular Wire. *Phys. Rev. B* **1998**, *57* (3), 1820.
(43) Lee, W.; Louie, S.; Evans, A. M.; Orchanian, N. M.; Stone, I. B.; Zhang, B.; Wei, Y.; Roy, X.; Nuckolls, C.; Venkataraman, L. Increased Molecular Conductance in Oligo[ n]Phenylene Wires by Thermally Enhanced Dihedral Planarization. *Nano Lett.* **2022**, *22* (12), 4919−4924.
(44) Lee, T.; Wang, W.; Reed, M. A. Mechanism of Electron Conduction in Self-Assembled Alkanethiol Monolayer Devices. *Ann. N. Y. Acad. Sci.* **2003**, *1006*, 21−35.
(45) Choi, S. H.; Risko, C.; Delgado, M. C. R.; Kim, B.; Bredas, J.-L.; Frisbie, C. D. Transition from Tunneling to Hopping Transport in Long, Conjugated Oligo-Imine Wires Connected to Metals. *J. Am. Chem. Soc.* **2010**, *132* (12), 4358−4368.
(46) Choi, S. H.; Kim, B.; Frisbie, C. D. Electrical Resistance of Long Conjugated Molecular Wires. *Science (80-.)* **2008**, *320* (5882), 1482−1486.
(47) Stendardo, E.; Pedone, A.; Cimino, P.; Cristina Menziani, M.; Crescenzi, O.; Barone, V. Extension of the AMBER Force-Field for the Study of Large Nitroxides in Condensed Phases: An Ab Initio Parameterization. *Phys. Chem. Chem. Phys.* **2010**, *12* (37), 11697−11709.
(48) Pracht, P.; Bohle, F.; Grimme, S. Automated Exploration of the Low-Energy Chemical Space with Fast Quantum Chemical Methods. *Phys. Chem. Chem. Phys.* **2020**, *22* (14), 7169−7192.
(49) Grimme, S. Exploration of Chemical Compound, Conformer, and Reaction Space with Meta-Dynamics Simulations Based on Tight-Binding Quantum Chemical Calculations. *J. Chem. Theory Comput.* **2019**, *15* (5), 2847−2862.
(50) Herrmann, C.; Solomon, G. C.; Subotnik, J. E.; Mujica, V.; Ratner, M. A. Ghost Transmission: How Large Basis Sets Can Make Electron Transport Calculations Worse. *J. Chem. Phys.* **2010**, *132* (2), 024103.
(51) Steenbock, T.; Tasche, J.; Lichtenstein, A. I.; Herrmann, C. A Green's-Function Approach to Exchange Spin Coupling As a New Tool for Quantum Chemistry. *J. Chem. Theory Comput.* **2015**, *11* (12), 5651−5664.
(52) Lu, T.; Chen, F. Multiwfn: A Multifunctional Wavefunction Analyzer. *J. Comput. Chem.* **2012**, *33* (5), 580−592.
(53) Chi, T.; Akkiraju, S.; Liang, Z.; Tan, Y.; Kim, H. J.; Zhao, X.; Savoie, B. M.; Boudouris, B. W. Design of an N-Type Low Glass Transition Temperature Radical Polymer. *Polym. Chem.* **2021**, *12* (10), 1448−1457.
(54) Kemper, T. W.; Larsen, R. E.; Gennett, T. Relationship between Molecular Structure and Electron Transfer in a Polymeric Nitroxyl-Radical Energy Storage Material. *J. Phys. Chem. C* **2014**, *118* (31), 17213−17220.


https://doi.org/10.1021/acs.nanolett.3c00978
*Nano Lett.* 2023, 23, 5951−5958